Theor Chem Account (2008) 121:135–146
DOI 10.1007/s00214-008-0456-1

REGULAR ARTICLE

Theoretical study of N–H· · · O hydrogen bonding properties and cooperativity effects in linear acetamide clusters

Mehdi D. Esrafili · Hadi Behzadi · Nasser L. Hadipour

Received: 13 February 2008 / Accepted: 7 May 2008 / Published online: 31 May 2008

Abstract We investigated geometry, energy, $\nu_{N–H}$ harmonic frequencies, ^{14}N nuclear quadrupole coupling tensors, and $n_O \rightarrow \sigma^*_{N–H}$ charge transfer properties of $(acetamide)_n$ clusters, with $n = 1-7$, by means of second-order Møller-Plesset perturbation theory (MP2) and DFT method. Dependency of dimer stabilization energies and equilibrium geometries on various levels of theory was examined. B3LYP/6-311++G** calculations revealed that for acetamide clusters, the average hydrogen-bonding energy per monomer increases from $-26.85\,kJ\,mol^{-1}$ in dimer to $-35.12\,kJ\,mol^{-1}$ in heptamer; i.e., 31% cooperativity enhancement. The n-dependent trend of $\nu_{N–H}$ and ^{14}N nuclear quadrupole coupling values were reasonably correlated with cooperative effects in $r_{N–H}$ bond distance. It was also found that intermolecular $n_O \rightarrow \sigma^*_{N–H}$ charge transfer plays a key role in cooperative changes of geometry, binding energy, $\nu_{N–H}$ harmonic frequencies, and ^{14}N electric field gradient tensors of acetamide clusters. There is a good linear correlation between ^{14}N quadrupole coupling constants, $C_Q(^{14}N)$, and the strength of Fock matrix elements (F_{ij}). Regarding the $n_O \rightarrow \sigma^*_{N–H}$ interaction, the capability of the acetamide clusters for electron localization, at the N–H· · · O bond critical point, depends on the cluster size and thereby leads to cooperative changes in the N–H· · · O length and strength, N–H stretching frequencies, and ^{14}N quadrupole coupling tensors.

M. D. Esrafili · H. Behzadi · N. L. Hadipour (✉)
Department of Chemistry, Tarbiat Modares University,
P.O. Box 14115-175, Tehran, Iran
e-mail: hadipour@modares.ac.ir; nas.hadipour@gmail.com

N. L. Hadipour
Institute of Chemistry, Academia Sinica,
Nankang, Taipei 11529, Taiwan, ROC

Keywords Hydrogen-bonding cooperativity · DFT · ^{14}N quadrupole coupling tensors · Acetamide · NBO · AIM

1 Introduction

One particularly relevant aspect in the hydrogen bonding theory is hydrogen-bond *cooperativity*, which is typically described as nonadditive enhancement of a hydrogen bond through formation of another hydrogen bond with either a proton donor or proton acceptor [1–8]. In other words, due to the nonadditive character of the polarization effects involved in hydrogen bonding, H-bonding, structure and electronic properties of the aggregates are mostly dependent on number of monomers in the cluster. On the other hand, it is expected that for clusters larger than a size limit n, the importance of these effects be noticeably reduced. Considerable attention has been given to cooperative effects of hydrogen-bonding chains in molecular clusters. For example, Weinhold et al. [9,10] employed reasonably high levels of ab initio theory to investigate cooperative aspects of C–H· · · N H-bonding in $(HCN)_{n=1-7}$ clusters. Their results indicated that cooperative effects are robust and pervasive in $(HCN)_n$ clusters, extending to virtually every aspect of energetic, structural, dielectric and vibrational properties. The ab initio study performed by Parra and coworkers [11,12] revealed existence of significant cooperative effects in a linear network of three-centered bifurcated A_1 HA $_2$hydrogen bond. They also indicated that cooperative effects play a significant role in stabilization of ring-like network containing bifurcated $H_1 \cdots A \cdots H_2$ H-bonding interaction, where the two proton-donors are located in the same molecules. On the basis of density functional theory studies, Ludwig et al. [3,4] found strong cooperative effects in linear clusters of *trans-N*-methylamide using quantum cluster equilibrium (QCE) methodology and

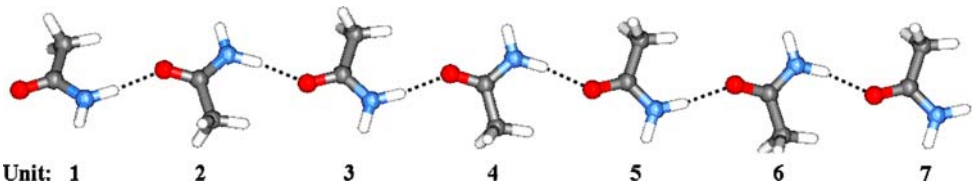

Fig. 1 Optimized geometry for the gas-phase $(acetamide)_7$ cluster

suggested the possibility to extend this method for a vast spectrum of other H-bonded liquids. Dannenberg et al. [13] reported an unusually high degree of cooperativity in hydrogen bond chains of formamide and their implications in protein modeling. Kar and Scheiner [14] have just recently conducted a comparative study of the cooperativity in C–H$\cdots$O and O–H$\cdots$O hydrogen bonds. This work presents the rather interesting result that the cooperativity of C–H$\cdots$O and O–H$\cdots$O bonds is similar, although solvent effects, represented by a continuum with a dielectric constant, result in reduced cooperativity in all systems.

Acetamide looks like a simple molecular model for the presence of N–H$\cdots$O hydrogen-bond cooperativity in gas-phase (Fig. 1). Owing to the importance of N–H$\cdots$O interaction in protein and polypeptides stability, acetamide has received most attention from the theoretical [15–18] and experimental [19–24] points of view. Recently, it has been widely indicated that formation of a supermolecular hydrogen-bonded cluster is accompanied by electron density redistribution. In some cases, this redistribution is so considerable that it leads to partial intermolecular charge transfer [25,26]. The amount of charge transferred between interacting molecules may affect corresponding intermolecular forces and, therefore, knowledge of this property could be critical in modeling various chemical processes [27]. Moreover, charge transfer between monomers plays an important role in biological processes [28]. The aim of this work is to systematically examine properties of N–H$\cdots$O interaction in various $(acetamide)_n$ clusters based on second order Møller-Plesset perturbation theory (MP2) and density functional theory (DFT). We will discuss the structural, energetical, vibrational and ^{14}N quadrupole coupling properties of the clusters, H-bonding cooperativity and its dependence on cluster size. We also indicate the role of $n_O \rightarrow \sigma^*_{N-H}$ charge transfer in cooperative changes of acetamide clusters.

2 Computational aspects

2.1 MP2 and DFT calculations

Molecular orbital calculations were performed using DFT and MP2 methods. All the computations were carried out using Gaussian 98 program [29]. The geometry optimization of monomer and dimer acetamide were performed with subsequent frequency calculations using the B3LYP, $PW91_{XC}$ and MP2 methods with 6-311+G*, 6-311++G**, cc-pVTZ and aug-cc-pVTZ basis sets. For the geometry optimization and vibrational frequency calculations of linear $(acetamide)_{3-7}$clusters, we only utilize the B3LYP [30,31] method with 6-311++G** basis set. Although geometries were not optimized, however, on the counterpoise-corrected (CP) surface [32], the interaction energies and the zero-point vibrational energy (ZPVE) corrections obtained at the MP2 and DFT levels were corrected for the basis set superposition error (BSSE) [32]. The BSSE corrected energies were determined by means of

$$\Delta E = E_n - \sum_i^n E_i \tag{1}$$

where E_n is the total energy of the cluster of size n, and E_i is the energy of the individual monomers, in the cluster geometry, calculated using all the basis set of the cluster. The MP2 correlation method was used in consideration of the results presented by Novoa and Sosa [33] suggesting that this method provides a better description of the energetics of H-bonded complexes than DFT methods.

It should be noted that a quantitative account of the cooperative effects can be achieved by decomposing the energy ΔE_n of an n-body system. Many-body decomposition scheme for binding energies employed by Hankins et al. [34], Xantheas [35] and Pedulla [36], for water clusters, and Almeida and coworkers [37], for hydrogen fluoride oligomers, reveal that interaction energies of H-bonded clusters may be separated into various n-body interactions which provides a detailed understanding of importance of the many-body interactions in these clusters. This knowledge has been essential for developing accurate analytical representations of the molecular potential energy surface.

^{14}N electric field gradient (EFG) calculations were performed using MP2/6-311++G** and B3LYP/6-311++G** levels of theory. The calculated EFG eigenvalues (q_{xx}, q_{yy} and q_{zz}) were used to obtain ^{14}N nuclear quadrupole coupling constant, $C_Q(\text{MHz}) = e^2 Q q_{zz}/h$, where e is the charge of electron, eQ is the nuclear electric quadrupole moment of the ^{14}N nucleus ($eQ_{14N} = 20.44\,\text{mb}$) and h is the Plank's constant [38]. The C_Q parameter is a measure of the interaction between the nuclear quadrupole moment and the EFG at the quadrupole nucleus site due to the nonspherical and noncylindrical (anisotropic) charge distribution in the system. Asymmetry parameter is another important parameter which

is a measure of the deviation of the charge distribution from axial symmetry, defined as: $\eta_Q = |(q_{yy} - q_{xx})/q_{zz}|, 0 \leq \eta_Q \leq 1$.

2.2 NBO calculations

Natural bonding orbital (NBO) analyses [39] were performed on wave functions calculated at the MP2/6-311++G** and B3LYP/6-311++G** levels. The NBO method corresponds closely to the picture of localized bonds and lone pairs as basic units of molecular structure. NBO analysis transforms the delocalized many-electron wave function into optimized electron pair bonding units, corresponding to the Lewis structure picture. Starting from a given input atomic orbital basis set $\{\chi_i\}$, the program performs a series of transformations to form "natural" atomic orbitals (NAOs), hybrid orbitals (NHOs), bond orbitals (NBOs), and semi-localized molecular orbitals (NLMOs). These orbitals are natural in the Löwdin sense [40], having optimal convergence properties for describing the electron density, ρ.

2.3 Atoms in molecules calculations

Atoms in molecules (AIM) analysis was performed using AIM 2000 code [41]. The bonding patterns of acetamide clusters can be reliably obtained from detailed analysis of electron density via its topographical study. In this analysis, critical points of electron density distribution (points at which $\nabla\rho = 0$ and $\nabla(\nabla^2\rho) = 0$) are obtained and additional characterization is done using the corresponding Hessian matrix (a 3×3 matrix of second derivatives). Diagonalization of this matrix yields the coordinate invariant eigenvalues: $\lambda_1 \leq \lambda_2 \leq \lambda_3$. The quantities Laplacian, $\nabla^2\rho_b$, of charge density at the bond critical point and ellipticity, ε, are defined as

$$\nabla^2\rho_b = \sum_{i=1}^{3} \lambda_i \tag{2}$$

$$\varepsilon = \frac{\lambda_1}{\lambda_2} - 1 \tag{3}$$

The negative Laplacian is an indicator of a covalent bond, whereas a positive Laplacian indicates a non-covalent interaction. The bond ellipticity is a measure of the stability and higher values indicate instability in the bond [42].

3 Results and discussion

3.1 Equilibrium geometries

Despite the large number of experimental [43,44] and theoretical studies [15,45,46] of acetamide, its structure has been controversial. Although the gas phase structure of acetamide has been determined by electron diffraction, no experimental information on the conformation of methyl group or the planarity of the amino group is available. Far infrared vapor-phase spectral studies of acetamide indicated that the amino group is very close to planar [47]. On the other hand, based on MP2 and configuration interaction with singles and doubles (CISD) levels, Wiberg and Wong [15] predicted an asymmetric conformation for acetamide both in the isolated state and in condensed phases. Since the planarity of acetamide is still unresolved, the potential energy surfaces of acetamide were examined both in C_1 and C_s symmetry. Full geometry optimizations have been performed along with analytic vibrational frequency calculations in order to characterize the structures obtained as minima on the potential energy surface.

The difference between the DFT and MP2 predictions about the NH2 moiety in acetamide molecule is noteworthy. B3LYP and $PW91_{XC}$ methods, at all basis set levels, show acetamide to be planar (in C_s symmetry), while MP2 calculations predict a nonplanar structure for the molecule (in the case of C_s constrained symmetry, an imaginary vibrational frequency corresponding to NH2 out-of-plane motion provides a signature for the nonplanar equilibrium geometry). These results clearly indicate that the planar structure of acetamide is not a local minimum on the MP2 electronic energy surface. Thus, all of the results we examined have C_1 symmetry.

The calculated structural parameters of monomer and dimer acetamide using the DFT and MP2 methods at 6-311+G*, 6-311++G**, cc-pVTZ and aug-cc-pVTZ basis sets are presented in Table 1. For the monomer acetamide, a general observation from comparing the calculated and experimental $r_{N–H}$ distances is that all calculated bond distances are slightly shorter than the experimental value ($r_{N–H} = 1.022$ Å) [43]. Furthermore, for a given method, addition of the diffuse and polarization functions into the basis set produces no significant influence in geometrical parameters. A similar result was noted in recent work on linear chains of formamide and carbonic acid molecules, in which a variety of basis sets at MP2 and DFT levels were employed [12,48]. Considering all geometric parameters obtained with different theoretical methods at different basis sets, the cc-pVTZ predicted bond lengths are relatively lower than other basis sets. The $r_{C=O}$ and $r_{C–N}$ values , calculated at MP2 level with 6-311++G** and cc-pVTZ basis sets, are in excellent agreement with experiment ($r_{C=O} = 1.220$ Å and $r_{C–N} = 1.380$ Å).

Surveying the calculated results, using the DFT and MP2 methods at different basis set levels reveals that changes in the monomer geometry are relatively considerable upon dimer formation. As in Table 1, dimer formation induces a small elongation of the $r_{N–H}$ and $r_{C=O}$ bonds involved in

Table 1 Calculated structural properties of monomer and dimer acetamide

Parameter	Method	6-311+G*	6-311++G**	cc-pVTZ	aug-cc-pVTZ	Exp.[a]
Monomer						
r_{N-H}	B3LYP	1.005	1.005	1.003	1.003	1.022
	$PW91_{XC}$	1.012	1.012	1.009	1.010	
	MP2	1.007	1.008	1.002	1.002	
$r_{C=O}$	B3LYP	1.218	1.218	1.216	1.217	1.220
	$PW91_{XC}$	1.227	1.227	1.224	1.226	
	MP2	1.222	1.221	1.220	1.222	
r_{C-N}	B3LYP	1.368	1.368	1.364	1.364	1.380
	$PW91_{XC}$	1.372	1.373	1.369	1.369	
	MP2	1.377	1.378	1.366	1.366	
Dimer						
r_{N-H}	B3LYP	1.013	1.014	1.013	1.011	–
	$PW91_{XC}$	1.023	1.025	1.023	1.022	
	MP2	1.013	1.015	1.012	1.013	
$r_{C=O}$	B3LYP	1.225	1.225	1.224	1.223	–
	$PW91_{XC}$	1.235	1.235	1.234	1.234	
	MP2	1.229	1.228	1.228	1.229	
r_{C-N}	B3LYP	1.361	1.361	1.359	1.358	–
	$PW91_{XC}$	1.365	1.365	1.365	1.362	
	MP2	1.370	1.371	1.361	1.362	
$r_{O\cdots H}$	B3LYP	1.992	1.987	1.978	1.987	–
	$PW91_{XC}$	1.952	1.937	1.928	1.936	
	MP2	2.012	1.992	1.941	1.942	
$\angle N-H\cdots O$	B3LYP	177.37	176.97	171.98	178.22	–
	$PW91_{XC}$	174.33	175.86	170.77	175.64	
	MP2	165.68	167.36	167.07	174.08	

Distances in angstroms. Angles in degrees

[a] Experimental values from Ref. [43]

hydrogen bond and a very small contraction of the r_{C-N} bond. A similar trend is present for other systems involving N–H$\cdots$O hydrogen bond [3,4,11,12]. For the theoretical levels employed here, the maximum r_{N-H} bond length change is calculated to be 0.011–0.014 Å for $PW91_{XC}$ at the four basis set levels. The main difference between the results provided by various methods was observed in the intermolecular distance between the atoms involved in hydrogen bond. Thus, with the 6-311+G*, the MP2 method provides distances about 0.06 Å, longer than those obtained with the $PW91_{XC}$ method, and the B3LYP method gave intermediate values. On the other hand, addition of diffuse and polarization functions to the 6-311+G* basis set shortens the hydrogen bond distance, whereas an opposite trend is observed for cc-pVTZ basis set. For the theoretical levels employed here, the N–H$\cdots$O angle is found to increase at the all basis set levels (with B3LYP> $PW91_{XC}$ >MP2 order).

Table 2 presents the calculated structural parameters for linear acetamide clusters at B3LYP/6-311++G** level. As is evident, cooperative effects lead to interesting geometries for the different acetamide clusters. Geometry changes are more prominent for the interior molecules, reflecting the influence of considerable cooperative effects. According to our results, an increase in r_{N-H} and $r_{C=O}$ bond lengths and a regular decrease in r_{C-N} is generally observed upon enlarging the size of cluster from monomer to heptamer. The relation between average r_{N-H} and $r_{C=O}$ bond distances in the linear acetamide clusters are obtained by a correlation (Fig. 2):

$$r_{N-H} = 0.8718 r_{C=O} - 0.057 \quad (R^2 = 0.998) \tag{4}$$

which suggests the N–H bond order be correlated with an increase in C=O bond distance. The n-dependence variations in either N–H and C=O bond distances can therefore serve as a good evidence for H-bond cooperativity in $(acetamide)_n$ clusters. The calculated r_{C-N} bond length for central molecule in heptamer model, 1.346 Å, differs from monomer value by 0.022 Å. On the other hand, it is evident from Table 2 that intermolecular O$\cdots$H bonds are also notably altered by the cooperative nature of hydrogen bond. It is seen that adding a third molecule reduce considerably $r_{N-H\cdots O}$ value by 0.085 Å. This distance increases by 6% from monomer to heptamer. The N–H$\cdots$O angle, 176.97°, is close to linear in dimer model. In the heptamer cluster, cooperative effects

Table 2 Structural properties of $(\text{acetamide})_{n=1-7}$ clusters calculated at B3LYP/6-311++G** level of theory

Parameter	$n=1$	$n=2$	$n=3$	$n=4$	$n=5$	$n=6$	$n=7$
$\mathbf{r}_{N-H}$	1.005	1.006	1.006	1.006	1.005	1.006	1.006
		1.014	1.015	1.016	1.016	1.016	1.016
			1.017	1.018	1.019	1.020	1.020
				1.018	1.019	1.020	1.021
					1.018	1.020	1.021
						1.017	1.020
							1.018
$\mathbf{r}_{C=O}$	1.218	1.223	1.224	1.225	1.225	1.225	1.225
		1.225	1.231	1.232	1.233	1.233	1.233
			1.226	1.232	1.234	1.235	1.235
				1.226	1.233	1.235	1.236
					1.227	1.233	1.235
						1.227	1.233
							1.227
$\mathbf{r}_{C-N}$	1.368	1.361	1.359	1.357	1.357	1.357	1.357
		1.360	1.358	1.350	1.349	1.349	1.349
			1.352	1.350	1.348	1.347	1.347
				1.359	1.349	1.347	1.346
					1.358	1.349	1.347
						1.358	1.349
							1.3589
$\mathbf{r}_{O\cdots H}$		1.987	1.951	1.937	1.933	1.931	1.930
			1.942	1.902	1.887	1.881	1.878
				1.930	1.885	1.872	1.866
					1.924	1.880	1.865
						1.925	1.877
							1.921
$\angle N-H\cdots O$		176.97	175.06	175.15	174.83	173.52	174.44
			173.41	173.07	171.98	171.55	171.61
				171.94	171.46	171.15	171.02
					172.44	171.37	171.014
						172.21	171.27
							172.21

between the acetamide clusters lead to 6° deviation from the dimer bond angle. Calculated cooperative effects in the acetamide chain can be compared with other hydrogen bonded systems. All above-mentioned results for acetamide clusters are compatible with those obtained at the DFT levels for formamide [48,49], *N*-methyl-formamide [50], polyalanine chains in α-helical and extended structure [51,52] and antiparallel β-sheet models [53].

3.2 Energetics

Table 3 presents the binding energy results for fully optimized dimer acetamide, provided by the three computational

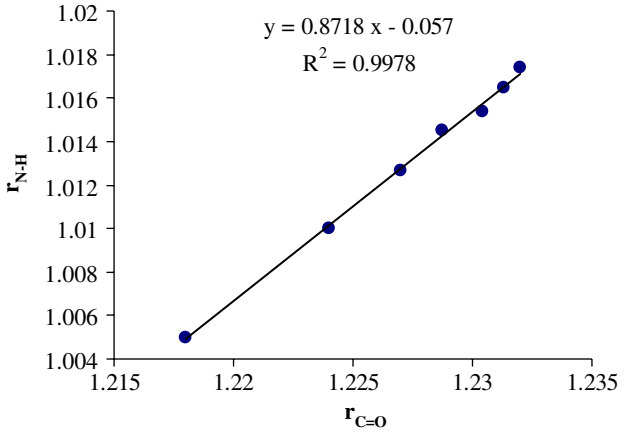

Fig. 2 B3LYP/6-311++G** calculated average r_{N-H} bond distances values versus $r_{C=O}$ in linear gas-phase $(\text{acetamide})_{n=1-7}$ clusters

Table 3 Binding energies, ΔE_e, ZPVE corrected binding energies, ΔE_0, and BSSE+ZPVE corrected binding energies, ΔE_0^{CP}, for $(\text{acetamide})_2$ clusters

Parameter	Method	6-311+G*	6-311++G**	cc-pVTZ	aug-cc-pVTZ
ΔE_e	B3LYP	−27.47	−26.85	−29.45	−25.57
	$PW91_{XC}$	−31.76	−31.22	−34.86	−29.85
	MP2	−33.38	−33.16	−37.17	−33.28
ΔE_0	B3LYP	−22.21	−21.88	−23.66	−20.69
	$PW91_{XC}$	−26.72	−26.17	−28.68	−24.53
	MP2	−29.28	−28.68	−31.36	−29.74
ΔE_0^{CP}	B3LYP	−21.92	−21.82	−22.21	−19.79
	$PW91_{XC}$	−26.41	−26.10	−27.94	−23.31
	MP2	−28.86	−28.56	−29.33	−27.21

All calculated energies in kJ mol^{-1}

methods (B3LYP, $PW91_{XC}$ and MP2) with the 6-311+G*, 6-311++G**, cc-pVTZ and aug-cc-pVTZ basis sets. Good agreement between our results and other theoretical predictions is also observed. For example, the ΔE_e value from $PW91_{XC}$/cc-pVTZ (−34.86 kJ mol^{-1}) is consistent with coupled-cluster (−35.38 kJ mol^{-1}) value reported by Davidson and White [54]. According to Table 3, different theories and basis sets have important effects on the interaction energies of the hydrogen bonding. Investigating the basis set dependence, we found that the diffuse and polarization functions, for both 6-311+G* and cc-pVTZ basis sets, lead to stabilization energy decrease. However, aug-cc-pVTZ calculations produce smallest binding energies among the others. It can be also observed from Table 3 that for the $(\text{acetamide})_2$ cluster, the ZPE and BSSE corrected binding energy, ΔE_0^{CP}, is found to be −21.92, −26.41 and −28.86 kJ mol^{-1}, with the smaller basis set, at the B3LYP, $PW91_{XC}$ and MP2 levels, respectively. The data are about 3.96 kJ mol^{-1} smaller than the only CP-corrected interaction

Table 4 Calculated binding energies, ΔE_e, association energies, $\Delta E_{e,n,n-1}$, and BSSE corrected binding energies, ΔE_e^{CP}, with 6-311++G** basis set for $(acetamide)_{n=2-7}$ clusters

Parameter	Method	$n=2$	$n=3$	$n=4$	$n=5$	$n=6$	$n=7$
ΔE_e	B3LYP	−26.85	−30.25	−32.26	−33.56	−34.46	−35.12
	MP2	−33.16	−35.03	−36.70	−37.76	−38.49	−39.17
$\Delta E_{e,n,n-1}$	B3LYP	−26.85	−33.64	−36.28	−37.47	−38.07	−38.40
	MP2	−33.16	−38.15	40.03	−40.94	−41.41	−42.59
ΔE_e^{CP}	B3LYP	−26.79	−30.12	−32.06	−33.28	−34.10	−34.60
	MP2	−33.06	−34.82	−36.35	−37.20	−37.96	−38.48
Cooperativity	B3LYP	–	3.33	5.27	6.49	7.31	7.81
	MP2	–	1.76	3.29	4.14	4.9	5.42

All calculated energies in kJ mol^{-1}

energy for formamide dimer calculated at the same theoretical levels [17]. On the other hand, stabilization energy of the dimer tends to decrease, by $\cong$ 0.1–0.5 kJ mol^{-1}, when a larger basis set containing second polarization and diffuse functions is adopted (6-311++G**). However, going from cc-pVTZ to aug-pVTZ basis set, a considerable difference in binding energy is observed to be about 2.50 kJ mol^{-1}, at the B3LYP and $PW91_{XC}$ levels. Furthermore, the effect of BSSE on the binding energies is quite selective. Since the BSSE introduces a nonphysical attraction between the monomers, the CP correction makes the chain less stable, which is observed to be larger for the MP2 calculations as compared to the DFT method.

Calculated H-bonding interaction energies of the fully optimized linear acetamide clusters, at the MP2/6-311++G** and B3LYP/6-311++G** levels of theory, are presented in Table 4. The deviation of the average binding energy from that of dimer is another indication of hydrogen bond cooperativity. Both MP2 and B3LYP calculations predict that for acetamide clusters, cooperative effects tend to increase intermolecular binding energies. Cooperative enhancement stabilizes the average H-bond interaction in the heptamer by about −35.12 and −39.17 kJ mol^{-1}, at the B3LYP and MP2 levels, which is equivalent to adding 8.27 and 7.25 kJ mol^{-1} to the dimer H-bonding energy, respectively. The ΔE_e is increased by 31% at the B3LYP and 18% at the MP2 levels of theory, which is smaller than the extrapolated percent increase in the one dimensional chains of formamide molecules (200%) [49] and urea molecules (55%) [55]. The ordering of cooperativity enhancement in the ΔE_e calculated for formamide (−54.32 kJ mol^{-1}) [49] and urea (−44.74 kJ mol^{-1}) [55] support the view that the degree of cooperativity is proportional to strength of N–H···O hydrogen bond.

Table 4 reveals also the energy changes by addition of one monomer to the $(acetamide)_{n-1}$ cluster according to acetamide + $(acetamide)_{n-1}$ → $(acetamide)_n$ reaction. It must be mentioned that with no-cooperative effects, energy of the process would have been constant and identical to the binding energy of the dimer. However, Table 4 predicts, at the B3LYP level, a 6.79 kJ mol^{-1} cooperative enhancement from dimer to trimer cluster which means a 25% increase with respect to the dimer binding energy. These cooperative effects become less significant by cluster enlargement.

The importance of BSSE correction on the cooperative effects was also studied. The magnitude of the BSSE can be judged by comparing the H-bonding energies, ΔE_0 , and corrected binding energy, ΔE_e^{CP}, values. As Table 4 indicates, at both levels of theory, the CP correction for all the cases is about 5–6% of the binding energies. Considering the values mentioned above, the percentage of cooperative enhancement would be quite similar for corrected and uncorrected values. Therefore, it can be concluded that BSSE has no important role in studying the cooperative effects.

3.3 N–H harmonic stretching frequencies

Vibrational frequency shifts are commonly used to gauge the cooperative nature of H-bonding interactions. Through the H-bonding interaction, N–H stretching frequency shifts to lower frequency, and its intensity increases. The amount of these changes depends on the strength of H-bonding interaction. Cooperative effects strengthen the H-bonding interactions and therefore lead to considerable shifts in frequency. Table 5 presents the calculated B3LYP/6-311++G** ν_{N-H} stretching frequencies of acetamide clusters. For the isolated acetamide molecule, the asymmetric ν_{N-H} frequency is detected at 3,728 cm^{-1}. According to Table 5, a convenient measure of harmonic frequency cooperativity is given as

$$\text{cooperativity} = \Delta\nu = [\langle\nu\rangle - \nu(\text{monomer})] \quad (5)$$

where $\Delta\nu$ is the amount of cluster frequency deviation from the monomer. For each cluster, average frequency shift $\Delta\nu$ is defined as the difference between average stretching frequency N–H of cluster$\langle\nu\rangle$ and the frequency of monomers. Although relative cooperative enhancement is largest for the trimer, further appreciable increases are still present in larger clusters (Table 5). As the chain becomes longer, the ν_{N-H} frequency vibration decreases markedly to 3,455 cm^{-1} in the chain of seven acetamides, a red shift of 90 cm^{-1} from that of dimer and 138 cm^{-1} from that of the monomer. This finding

Table 5 N–H stretching frequencies (in cm^{-1}) and average frequency shift relative to the monomer in $(acetamide)_{n=1-7}$ clusters

Frequency	$n=1$	$n=2$	$n=3$	$n=4$	$n=5$	$n=6$	$n=7$
ν_1	3,593	3,500	3,458	3,434	3,411	3,396	3,480
ν_2		3,590	3,487	3,451	3,428	3,414	3,380
ν_3			3,590	3,478	3,447	3,421	3,414
ν_4				3,589	3,476	3,452	3,410
ν_5					3,589	3,474	3,446
ν_6						3,589	3,472
ν_7							3,585
$\langle\nu\rangle$	3,593	3,545	3,512	3,488	3,470	3,458	3,455
$\Delta\nu$		48	81	105	118	130	133

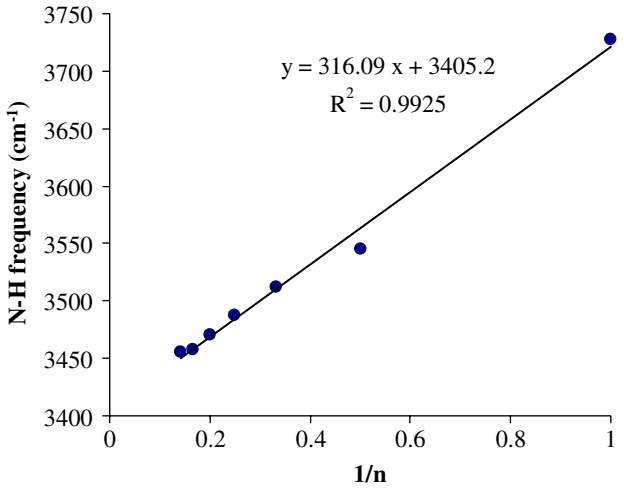

Fig. 3 Average ν_{N-H} frequencies (in cm^{-1}) for acetamide clusters versus $(1/n)$

is remarkably smaller than that reported for $(formamide)_{10}$ clusters (ca. 269 cm^{-1}deviation from monomer value) [56] revealing that cooperative effects in acetamide clusters are weaker than formamide. These trends are shown graphically in Fig. 3 where almost a perfect linear correlation between the frequencies and $1/n$ is obtained:

$$\nu_{N-H} = 316.09\left(\frac{1}{n}\right) + 3{,}405 \quad (R^2 = 0.9925) \tag{6}$$

where average ν_{N-H} approaches 3,405 cm^{-1} as $n \to \infty$. This value suggests a deviation of about 140 cm^{-1} from the dimer. Besides, calculated harmonic frequencies for acetamide clusters revealed that at B3LYP/6-311++G** level of theory, theoretical values overestimate experimental data (3,432 cm^{-1}) [57]. Our results for larger clusters are also in complete agreement with the equilibrium structural parameters and binding energies, in which H-bonding cooperativity decreases remarkably from gas-phase $(acetamide)_2$ to $(acetamide)_7$ cluster, but tends to reach an approximate limit for larger clusters.

Spectroscopic studies of acetamide clusters are frequently carried out in condensed phases, usually inert gas matrix. However, interaction with the matrix atoms may affect the vibrational structure of H-bonded complex [57]. There is also numerous evidence suggesting that these interactions modify the shape of intermolecular potential surface associated with vibrational motion [58]. As inferred from Table 5, the ν_{N-H} harmonic frequency for the heptamer cluster reasonably meets the available experimental data. The 23 cm^{-1} deviation from the experimental data can be partially related to the intrinsic limitation of DFT-based methods for calculation of harmonic frequencies. The presented results for $\Delta\nu$ in various acetamide clusters provide a clear illustration of H-bonding cooperativity which complements the equilibrium structures data and binding energies.

3.4 ^{14}N quadrupole coupling tensors

Table 6 shows the calculated MP2/6-311++G** and B3LYP/6-311++G** average ^{14}N EFG eigenvalues, their associated nuclear quadrupole coupling constants, $C_Q(^{14}N)$, and asymmetry parameters, η_Q, for acetamide clusters. For each acetamide cluster, the EFG values obtained by MP2 method overestimate B3LYP values. Calculation results are consistent with the experimental values reported for formamide molecule [59].

The intermolecular hydrogen bonds are expected to strongly affect electronic environment at the hydrogen-bonded nuclei. Thus, the cooperative effects in electronic structure induced by N–H···O hydrogen-bond formation influence the EFG properties of the ^{14}N nuclei in $(acetamide)_n$ clusters. According to Table 6, both B3LYP and MP2 methods predict that as the number of monomers in acetamide clusters increases, the calculated q_{zz}, and therefore C_Q, tends to decrease, whereas the η_Q shows an opposite trend. More specifically, at the B3LYP level, the $C_Q(^{14}N)$ value decreases from 4.49 MHz for the monomer to 3.99 MHz in the dimer (11%). Corresponding asymmetry parameter increases from 0.05 to 0.06 units in the same cluster. With increasing the cluster size, from dimer to heptamer cluster, the EFG eigenvalues receive a limit. The C_Q decreases by 20%, at the B3LYP level, and 19%, at the MP2 level, with the greatest jump of 0.93 MHz from dimer to trimer. This indicates that, in agreement with the previous sections, the cooperative effects on ^{14}N quadrupole coupling tensor decrease by increasing the number of monomers in the clusters.

3.5 Role of $n_O \to \sigma^*_{NH}$ interaction

In terms of NBO theory [60], A–H···B hydrogen bonding can be attributed to the localized $n_B \to \sigma^*_{AH}$ interaction due to electronic delocalization from the filled lone pair n(B) of "electron donor" B into the unfilled antibond σ^*(A–H) of

Table 6 ^{14}N EFG principal components, q_{ii}, nuclear quadrupole coupling constants, C_Q, and asymmetry parameters, η_Q, for (acetamide)$_{1-7}$ clusters

Parameter	Method	$n=1$	$n=2$	$n=3$	$n=4$	$n=5$	$n=6$	$n=7$	Exp.[a]
q_{xx}(au)	B3LYP	−0.445	−0.422	−0.315	−0.285	−0.257	−0.253	−0.243	−0.412
	MP2	−0.472	−0.448	−0.315	−0.306	−0.278	−0.273	−0.264	
q_{yy}(au)	B3LYP	−0.490	−0.476	−0.529	−0.493	−0.499	−0.498	−0.500	−0.390
	MP2	−0.520	−0.508	−0.530	−0.529	−0.535	−0.535	−0.536	
q_{zz}(au)	B3LYP	0.934	0.830	0.845	0.777	0.756	0.752	0.743	0.802
	MP2	0.992	0.956	0.845	0.835	0.813	0.808	0.800	
C_Q(MHz)	B3LYP	4.49	3.99	4.06	3.73	3.63	3.61	3.57	3.85
	MP2	4.77	4.59	4.06	4.01	3.91	3.88	3.84	
η_Q	B3LYP	0.05	0.06	0.25	0.27	0.32	0.33	0.35	0.03
	MP2	0.05	−0.07	−0.25	−0.27	−0.32	−0.32	−0.34	

[a] Experimental EFG values from microwave study, Ref. [59]

Table 7 NBO analysis of donor-acceptor interactions in (acetamide)$_{n=1-7}$ clusters showing Fock matrix interaction elements F_{ij}, stabilization $E(2)$ values, hybrid decompositions, energies ε (au), and occupancies (e) of n_O (oxygen lone pair) and σ^*_{N-H} (NH antibond) NBOs calculated at B3LYP/6-311++G** and MP2/6-311++G** levels

n	Method	F_{ij}	$E(2)$	Donor			Acceptor		
				n_O	ε_i	Occu.	σ^*_{NH}	ε_j	Occu.
1	B3LYP	–	–	$sp^{0.68}$	−0.680	1.978	$0.30sp^{2.36}$–0.70 s	0.412	0.009
	MP2	–	–	$sp^{0.70}$	−0.929	1.979	$0.30sp^{2.35}$–0.70 s	0.676	0.007
2	B3LYP	0.062	4.09	$sp^{0.69}$	−0.709	1.970	$0.28sp^{2.04}$–0.72 s	0.469	0.023
	MP2	0.078	4.50	$sp^{0.71}$	−0.958	1.974	$0.30sp^{2.26}$–0.70 s	0.739	0.005
3	B3LYP	0.067	4.78	$sp^{0.69}$	−0.685	1.968	$0.28sp^{2.01}$–0.72 s	0.482	0.027
	MP2	0.085	5.37	$sp^{0.70}$	−0.933	1.972	$0.27sp^{2.02}$–0.73 s	0.752	0.018
4	B3LYP	0.076	6.18	$sp^{0.69}$	−0.694	1.966	$0.27sp^{2.01}$–0.73 s	0.464	0.028
	MP2	0.096	6.91	$sp^{0.71}$	−0.942	1.971	$0.27sp^{2.02}$–0.73 s	0.733	0.019
5	B3LYP	0.077	6.50	$sp^{0.70}$	−0.683	1.965	$0.27sp^{2.00}$–0.73 s	0.469	0.030
	MP2	0.099	7.31	$sp^{0.71}$	−0.932	1.970	$0.27sp^{2.01}$–0.73 s	0.739	0.020
6	B3LYP	0.079	6.83	$sp^{0.70}$	−0.688	1.964	$0.27sp^{2.00}$–0.73 s	0.461	0.032
	MP2	0.101	7.71	$sp^{0.71}$	−0.937	1.969	$0.27sp^{2.01}$–0.73 s	0.730	0.021
7	B3LYP	0.080	6.93	$sp^{0.70}$	−0.682	1.964	$0.27sp^{1.99}$–0.73 s	0.463	0.032
	MP2	0.102	7.85	$sp^{0.71}$	−0.931	1.969	$0.27sp^{2.00}$–0.73 s	0.733	0.022

"electron acceptor" A–H. Stabilization energy, $E(2)$, reflects the attractive interaction in the A–H$\cdots$B bonding and thus can be used to characterize the strength of the A–H$\cdots$B bond. For each electron donor NBO(i) and acceptor NBO(j), $E(2)$ associated with delocalization $i \rightarrow j$ is estimated as

$$E(2) = \Delta E_{ij} = q_i \frac{F_{ij}^2}{\varepsilon_j - \varepsilon_i} \tag{7}$$

where q_i is donor orbital occupancy, ε_i and ε_j are orbital energies, and F_{ij} is the off-diagonal NBO Fock matrix element.

Table 7 shows considerable cooperativity in some characteristics of n_O, σ^*_{N-H} NBOs (energy, occupation, and hybridization), $E(2)$ and Fock matrix elements (F_{ij}) along the different (acetamide)$_n$ clusters. The calculated delocalization energy for $n_O \rightarrow \sigma^*_{NH}$ interaction of dimer is 4.09 and 4.50 kcal mol^{-1}, at the B3LYP and MP2 levels, respectively. This energy increases to 4.78 and 5.37 kcal mol^{-1} in trimer, which is in accordance with other evidences for intermolecular hydrogen bond strength increase. It is expected that interior acetamide units of general N–H$\cdots$O=CNH$\cdots$N–H chain be left approximately electroneutral by simultaneous charge-transfer. When a small quantity of charge is transferred between the two acetamide molecules, in No.1 $\rightarrow$ No.2 sense, molecule No.2 acquires slight anionic character. This raises the energy of its filled orbitals and renders them

more spatially diffuse. On the other hand, the No.1 molecule acquires slight cationic property, rendering it better acceptor. Furthermore, the acceptor No.2, in No.1 → No.2 interaction, inherently becomes an improved donor for concerted No.1→No.2→ No.3 interactions.

It is worth mentioning that electron density transferred from the electron donor subunit to antibonding σ^* orbital of the electron acceptor, is often used to explain the elongations, red-shift of the N–H frequency, and down-shift of $C_Q(^{14}\mathrm{N})$ values in N–H···O. The NBO analysis (presented in Table 7) reveals an increase in $\sigma^*_{\mathrm{N–H}}$ population with cluster size. Increase in the electron population of $\sigma^*_{\mathrm{N–H}}$ orbital weakens the $r_{\mathrm{N–H}}$ bond, which reflected as a down-shift in $C_Q(^{14}\mathrm{N})$ values and a red-shift in the N–H stretch frequency.

As discussed in literatures, the characteristic property of N–H···O hydrogen bonding is closely associated with the fundamental $n_{\mathrm{O}} \rightarrow \sigma^*_{\mathrm{N–H}}$ Fock matrix elements (F_{ij}) that control intermolecular donor-acceptor interactions. As in Fig. 4a, shifts in calculated $C_Q(^{14}\mathrm{N})$ values are approximately proportional to $n_{\mathrm{O}} \rightarrow \sigma^*_{\mathrm{N–H}}$ Fock matrix elements. Thus, variation of $C_Q(^{14}\mathrm{N})$ allows a virtually direct measurement for $n_{\mathrm{O}} \rightarrow \sigma^*_{\mathrm{NH}}$ charge transfer along acetamide chains. Another correlation of $C_Q(^{14}\mathrm{N})$ with NBO quantities can be obtained from the occupancy of $\sigma^*_{\mathrm{N–H}}$ along the chains. Since each $\sigma^*_{\mathrm{N–H}}$ NBO is incrementally populated through the $n_{\mathrm{O}} \rightarrow \sigma^*_{\mathrm{N–H}}$ interactions, its occupancy should be a direct measure of the electronic shifts affecting $C_Q(^{14}\mathrm{N})$. Figure 4b indicates a reasonable linear correlation between the $C_Q(^{14}\mathrm{N})$ and $\sigma^*_{\mathrm{N–H}}$ values.

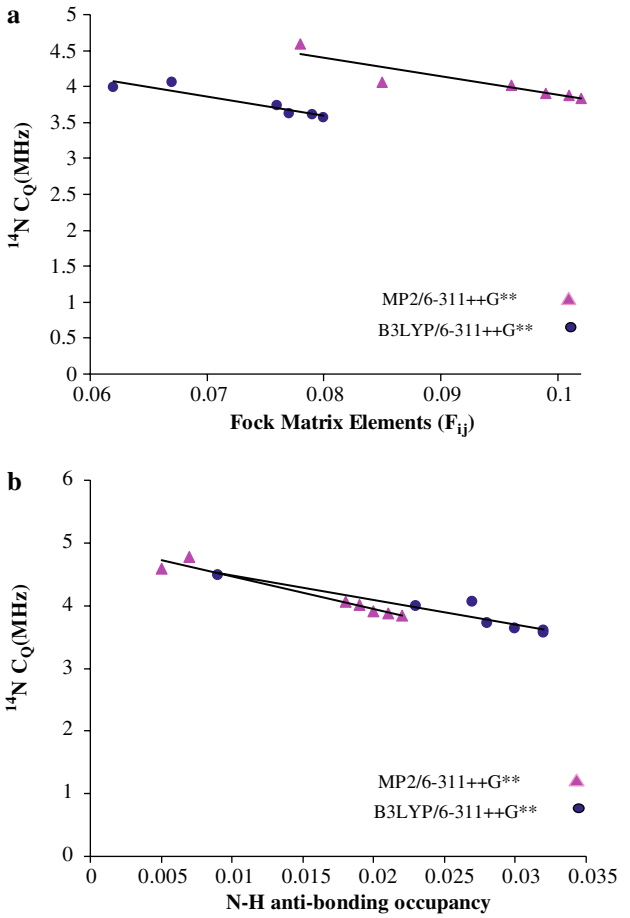

Fig. 4 Correlation of calculated $C_Q(^{14}\mathrm{N})$ quadrupole coupling constants of acetamide clusters versus **a** NBO $n_{\mathrm{O}} \rightarrow \sigma^*_{\mathrm{N–H}}$ charge transfer Fock matrix elements, and **b** occupancy of σ^*_{NH} antibond NBO (see text for description of individual plots)

3.6 Atoms in molecules analysis

Based on the AIM theory, properties of BCP serve to summarize the nature of the interaction between two atoms as shared (covalent) or closed-shell (ionic) interaction. The value of ρ at a BCP, $\rho_b(\mathbf{r}_{\mathrm{cp}})$, gives a loose indication of bond strength. Bader found a linear relationship between electron charge density value at hydrogen bond critical point and hydrogen bond strength as well as the intermolecular bond length [61].

Table 8 gives the λ_i, $\rho_b(\mathbf{r}_{\mathrm{cp}})$, ∇^2_ρ $(\mathbf{r}_{\mathrm{CP}})$ and ε values for $(\mathrm{acetamide})_{n=2-7}$ clusters. In accordance with the previous studies [42], the positive $\nabla^2_\rho(\mathbf{r}_{\mathrm{cp}})$ value has the same order of magnitude as $\rho(\mathbf{r}_{\mathrm{cp}})$ ($\sim 10^{-2}$ au), indicating that the intermolecular N–H···O bonds have the general characteristics of the hydrogen bond. The $\rho_b(\mathbf{r}_{\mathrm{cp}})$ at the N–H···O BCPs are all in the proposed range of 0.021–0.026 au and 0.020–0.028 au, at the B3LYP and MP2 levels, respectively. The corresponding $\nabla^2_\rho(\mathbf{r}_{\mathrm{cp}})$ values are in the range 0.083–0.108 au at the B3LYP and 0.088–0.115 au at the MP2 level of theory. The B3LYP estimated average $\rho_b(\mathbf{r}_{\mathrm{cp}})$ values for n=2–7 are 0.0214, 0.0226, 0.0258, 0.0268, 0.0279, 0.0284 au,

Table 8 Average BCP properties (calculated at B3LYP/6-311++G** and MP2/6-311++G** levels) for N–H···O hydrogen-bonding in acetamide clusters

n	Method	λ_1	λ_2	λ_3	$\rho_b(r_{\mathrm{CP}})$	$\nabla^2\rho(r_{\mathrm{CP}})$	ε
2	B3LYP	−0.0277	−0.0271	0.1381	0.0214	0.0833	0.0221
	MP2	−0.0253	−0.0246	0.1381	0.0196	0.0882	0.0285
3	B3LYP	−0.0300	−0.0293	0.1500	0.0226	0.0907	0.0239
	MP2	−0.0274	−0.0264	0.1498	0.0208	0.0960	0.0379
4	B3LYP	−0.0357	−0.0349	0.1710	0.0258	0.1004	0.0229
	MP2	−0.0327	−0.0315	0.1710	0.0237	0.1068	0.0381
5	B3LYP	−0.0377	−0.0367	0.1780	0.0268	0.1036	0.0272
	MP2	−0.0346	−0.0331	0.1780	0.0246	0.1103	0.0453
6	B3LYP	−0.0398	−0.0387	0.1851	0.0279	0.1066	0.0284
	MP2	−0.0358	−0.0344	0.1851	0.0254	0.1149	0.0410
7	B3LYP	−0.0408	−0.0397	0.1884	0.0284	0.1079	0.0277
	MP2	−0.0374	−0.0358	0.1885	0.0261	0.1153	0.0447

All λ_i, $\rho_b(\mathbf{r}_{\mathrm{cp}})$, $\nabla^2_\rho(\mathbf{r}_{\mathrm{cp}})$ values in atomic unit

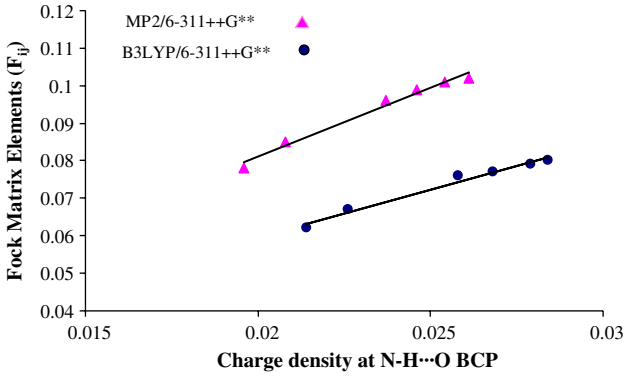

Fig. 5 Correlation of calculated $n_O \rightarrow \sigma^*_{N-H}$ charge transfer Fock matrix elements (F_{ij}) with charge density at N–H···O bond critical point of acetamide clusters

respectively. Clearly, the average value of $\rho_b(\mathbf{r}_{cp})$ for the heptamer is 1.33 times of the dimer. It can be concluded that the capacity of acetamide clusters to concentrate electrons at the N–H···O BCP increases with the cluster size which is consistent with F_{ij} values. In fact, according to F_{ij} and $\rho_b(\mathbf{r}_{cp})$ of N–H···O, an acceptable linear relation between the two physical quantities is observed at B3LYP and MP2 levels (Fig. 5):

$$\text{B3LYP:} \quad F_{ij}(\text{au}) = 2.5104\rho_b(r_{CP}) + 0.0095 \quad (R^2 = 0.977) \tag{8}$$

$$\text{MP2:} \quad F_{ij}(\text{au}) = 3.7132\rho_b(r_{CP}) + 0.0067 \quad (R^2 = 0.982) \tag{9}$$

These correlations indicate that the two representations of N–H···O strengths, based upon NBO and AIM, are approximately equivalent. Thereby, regarding the cooperativity of $n_O \rightarrow \sigma^*_{N-H}$ interaction, we believe that the capacity of the linear acetamide clusters, to concentrate electrons at the NH···O BCP, is sensitive to the cluster size, as is also reflected in the fact that the average value of $\rho_b(\mathbf{r}_{cp})$ (0.0284 au) for the heptamer is 1.33 times that for the dimer (0.0214 au).

4 Conclusion

This work reports MP2, DFT, NBO and AIM theories to investigate properties of N–H···O hydrogen bonding in linear H-bonded acetamide clusters ($n = 2-7$) such as equilibrium geometries, binding energies, N–H harmonic frequencies, ^{14}N EFG tensor, $n_O \rightarrow \sigma^*_{N-H}$ charge transfer, and AIM properties. It is obtained that the interaction energies of dimer acetamide depend considerably on the level of theory. We found 3.33 kJ mol^{-1} more stability in trimer cluster, at the B3LYP/6-311++G** level of theory, due to formation of the second hydrogen bond. Our calculations indicate that, as cluster size increases, the calculated N–H frequencies and $C_Q(^{14}N)$ parameters shift to lower values. The calculated delocalization energy of $n_O \rightarrow \sigma^*_{N-H}$ interaction increases with number of acetamide molecules in the cluster. It can be also concluded that the capacity of acetamide clusters to concentrate electrons at the N–H···O BCP increases with the cluster size. Such cooperative effects help rationalize the common occurrence of N–H···O type H-bonding interactions in the biosystems.

References

1. Del Bene JE, Pople JA (1969) Intermolecular energies of small water polymers. Chem Phys Lett 4:426–428
2. Clementi E, Kolos W, Lie GC, Ranghino G (1980) Nonadditivity of interaction in water trimers. Int J Quantum Chem 17:377–398
3. Ludwig R, Weinhold F, Farrar TC (1997) Structure of liquid *N*-methylacetamide: temperature dependence of NMR chemical shifts and quadrupole coupling constants. J Phys Chem A 101:8861–8870
4. Ludwig R, Weinhold F, Farrar TC (1997) Theoretical study of hydrogen bonding in liquid and gaseous *N*-methylformamide. J Chem Phys 107:499–507
5. Suhai S (1994) Cooperative effects in hydrogen-bonding 4th-order many body perturbation theory studies of water oligomers and of an infinite water chain as a model for ice. J Chem Phys 101:9766–9782
6. Xia QY, Xiao HM, Ju XH, Gong XD (2003) DFT study on cooperativity in the interactions of hydrazoic acid clusters. Int J Quantum Chem 94:279–286
7. Tan H, Qu W, Chen G, Liu R (2005) The role of charge transfer in the hydrogen bond cooperative effect of *cis-N*-methylfortnamide oligomers. J Phys Chem A 109:6303–6317
8. van Mourik T, Dingley AJ (2007) Characterizing the cooperativity in H-bonded amino structures. J Phys Chem A 111:11350–11358
9. King BF, Weinhold F (1995) Structure and spectroscopy of $(HCN)_n$ clusters-cooperative and electronic delocalization effects in C–H···N hydrogen-bonding. J Chem Phys 103:333–347
10. King BF, Farrer TC, Weinhold F (1995) Quadrupole coupling constants in linear $(HCN)_n$ clusters: theoretical and experimental evidence for cooperativity effects in C–H···N hydrogen bonding. J Chem Phys 103:348–352
11. Parra RD, Bulusu S, Zeng XC (2003) Cooperative effects in one-dimensional chains of three-center hydrogen bonding interactions. J Chem Phys 118:3499–3509
12. Parra RD, Bulusu S, Zeng XC (2005) Cooperative effects in two-dimensional ring-like networks of three-center hydrogen bonding interactions. J Chem Phys 122:184325–184328
13. Kobko N, Paraskevas L, del Rio E, Dannenberg JJ (2001) Cooperativity in amide hydrogen bonding chains: implications for protein-folding models. J Am Chem Soc 123:4348–4349
14. Karr T, Scheiner S (2004) Comparison of Cooperativity in CH···O and OH···O hydrogen bonds. J Phys Chem A 108:9161
15. Wong MW, Wiberg KB (1992) Structure of acetamide: planar or nonplanar. J Phys Chem 96:668–671
16. Hirst JD, Hirst DM, Brooks CL (1997) Multireference configuration interaction calculations of electronic states of *N*-methylformamide, acetamide, and *N*-methylacetamide. J Phys Chem A 101:4821–4827
17. Papamokos GV, Demetropoulos IN (2004) Vibrational frequencies of amides and amide dimers: the assessment of PW91(xc) functional. J Phys Chem A 108:7291–7300

18. Chipot C, Millot C, Maigret B, Kollman PA (1994) Molecular-dynamics free-energy simulation—infinite of the truncation of long-range nonbonded electrostatic interactions on free-energy calculations of polar-molecules. J Chem Phys 101:7953–7962
19. Nasr S, Bellissent-Funel MC, Cortes R (1999) X-ray and neutron scattering studies of liquid formic acid DCOOD at various temperatures and under pressure. J Chem Phys 110:10487–10952
20. Williams JC, McDermott AE (1993) *Cis-trans* energetics in urea and acetamide studied by deuterium NMR. J Phys Chem 97:12393–12398
21. Ferris TD, Lee PT, Farrar TC (1997) Synthesis of propiolamide and H-1, C-13 and N-15 NMR spectra of formamide, acetamide and propiolamide. Mag Reson Chem 35:571–576
22. Jeffrey GA, Ruble JR, McMullan RK, DeFrees DJ, Pople JA (1980) Neutron diffraction study at 23 K and ab initio molecular orbital studies of acetamide. Acta Crystallogr B 36:2292–2299
23. Knudsen R, Sala O, Hase Y (1994) A low temperature matrix isolation infrared study of acetamides. II: Thioacetamide and some deuterated derivatives. J Mol Struct 321:197–203
24. Bats JW, Haberecht MC, Wagner M (2003) A new refinement of the orthorhombic polymorph of acetamide. Acta Crystallogr E 59:1483–1485
25. Fiacco DL, Toro A, Leopold KR (2000) Structure, bonding, and dipole moment of $(CH_3)_3N–SO_3$. A microwave study. Inorg Chem 39:37–43
26. Hunt SW, Leopold KR (2001) Molecular and electronic structure of $C_5H_5N–SO_3$: correlation of ground state physical properties with orbital energy gaps in partially bound Lewis acid-base complexes. J Phys Chem A 105:5498–5506
27. van der Vaart A, Merz KM (1999) The role of polarization and charge transfer in the solvation of biomolecules. J Am Chem Soc 121:9182–9190
28. Van der Vaart A, Merz KM (2000) Charge transfer in biologically important molecules: comparison of high-level ab initio and semi-empirical methods. Int J Quantum Chem 77:27–43
29. Frisch MJ, Trucks GW, Schlegel HB, Scuseria GE, Robb MA, Cheeseman JR, Zakrzewski VG, Montgomery JA, Stratmann RE, Burant JC, Dapprich S, Millam JM, Daniels AD, Kudin KN, Strain MC, Farkas O, Tomasi J, Barone V, Cossi M, Cammi R, Mennucci B, Pomelli C, Adamo C, Clifford S, Ochterski J, Petersson GA, Ayala PY, Cui Q, Morokuma K, Malick DK, Rabuck AD, Raghavachari K, Foresman JB, Cioslowski J, Ortiz JV, Baboul AG, Stefanov BB, Liu G, Liashenko APiskorz P, Komaromi I, Gomperts R, Martin RL, Fox DJ, Keith T, Al-Laham MA, Peng CY, Nanayakkara A, Gonzalez C, Challacombe M, Gill PMW, Johnson B, Chen W, Wong MW, Andres JL, Gonzalez C, Head-Gordon M, Replogle ES, Pople JA (1998) Gaussian 98, Gaussian Inc., Pittsburgh, P B
30. Becke AD (1988) Density-functional exchange-energy approximation with correct asymptotic behavior. Phys Rev A 38:3098–3100
31. Lee C, Yang W, Parr RG (1988) Development of the Colle-Salvetti correlation-energy formula into a functional of the electron density. Phys Rev B 37:785–789
32. Boys SF, Bernardi F (1970) The calculation of small molecular interactions by the differences of separate total energies. Some procedures with reduced errors. Mol Phys 19:553–566
33. Novoa JJ, Sosa C (1995) Evaluation of the density functional approximation on the computation of hydrogen bond interactions. J Phys Chem 99:15873–15878
34. Hankins D, Moskowitz JW, Stillinger FH (1970) Water molecule interactions. J Chem Phys 53:4544–4554
35. Xantheas SS (2000) Cooperativity and hydrogen bonding network in water clusters. Chem Phys 258:225–231
36. Pedulla JM, Vila F, Jordan KD (1996) Binding-energy of the ring form of $(H_2O)(6)$—comparison of the predictions of conventional and localized-orbital Mp2 calculations. J Chem Phys 105:11091–11099
37. Rincón L, Almeyda R, Aldea DG (2005) Many-body energy decomposition analysis of cooperativity in hydrogen fluoride clusters. Int J Quantum Chem 102:443–453
38. Bersohn R (1952) Nuclear electric quadrupole spectra in solids. J Chem Phys 20:1505–1509
39. Foster JP, Weinhold F (1980) Natural hybrid orbitals. J Am Chem Soc 102:7211–7218
40. Löwdin P.-O (1955) Quantum theory of many-particle systems. I. Physical interpretations by means of density matrices, natural spin-orbitals, and convergence problems in the method of configurational interaction. Phys Rev 97:1474–1489
41. Biegler-Konig F, Schonbohm J, Bayles D (2001) Software news and updates—AIM2000—a program to analyze and visualize atoms in molecules. J Comput Chem 22:545–559
42. Bader RFW (1990) Atoms in molecules—a quantum theory. Oxford University Press, New York
43. Kitano M, Kuchtsu K (1973) Molecular structure of acetamide as studied by gas electron diffraction. Bull Chem Soc Jpn 46:3048–3051
44. Jeffrey GA, Ruble JR, McMullan RK, De Frees DJ, Binkley JS, Pople JA (1980) Neutron diffraction at 23 K and ab initio molecular-orbital studies of the molecular structure of acetamide. Acta Crystallogr B 36:2292–2299
45. Klimkowski VJ, Sellers HL, Schafer L (1979) Ab initio equilibrium geometry and conformational analysis of acetamide. J Mol Struct 54:299–301
46. Samdal S (1998) Acetamide, a challenge to theory and experiment? On the molecular structure, conformation, potential to internal rotation of the methyl group and force fields of free acetamide as studied by quantum chemical calculations. J Mol Struct 440:165
47. Hansen EL, Larsen NW, Nicolaisen M (1980) An infrared investigation of formamide, acetamide, and thiocetamide in the vapour phase Inversion of the amino group. Chem Phys Lett 69:327
48. Vargas R, Garza J, Friesner RA, Stern H, Hay BP, Dixon DA (2001) Strength of the N–H$\cdots$O=C and C–H$\cdots$O=C bonds in formamide and *N*-methylacetamide. J Phys Chem A 105:4963–4968
49. Kobko N, Dannenberg JJ (2003) Cooperativity in amide hydrogen bonding chains. Relation between energy, position, and H-bond chain length in peptide and protein folding models. J Phys Chem A 107:10389–10395
50. Martínez AG, Vilar ET, Fraile G, Martínez-Ruiz P (2006) Density functional study of self-association of *n*-methylformamide and its effect on intramolecular and intermolecular geometrical parameters and *cis*/*trans* population. J Chem Phys 124:23435–23440
51. Ireta J, Neugebauer J, Scheffler M, Rojo A, Galván M (2003) Density functional theory study of the cooperativity of hydrogen bonds in finite and infinite r-helices. J Phys Chem B 107:1432–1437
52. Wieczorek R, Dannenberg JJ (2003) H-bonding cooperativity and energetics of α-helix formation of five 17-amino acid peptides. J Am Chem Soc 125:8124–8129
53. Viswanathan R, Asensio A, Dannenberg JJ (2004) Cooperative hydrogen-bonding in models of anti-parallel β-sheets. J Phys Chem A 108:9205–9212
54. White JC, Davidson ER (1993) Comparison of ab initio and multipole determinations of the electrostatic interaction of acetamide dimmers. J Mol Struct Theochem 282:19–31
55. Masunov A, Dannenberg JJ (2000) Theoretical study of urea and thiourea. 2. Chains and ribbons. J Phys Chem B 104:806–810
56. Kobko N, Dannenberg JJ (2003) Cooperativity in amide hydrogen bonding chains. A comparison between vibrational coupling through hydrogen bonds and covalent bonds. Implications for peptide vibrational spectra. J Phys Chem B 107:6688–6697

57. Knudsen R, Sala O, Hase Y (1994) A low temperature matrix isolation infrared study of acetamides. I. Acetamide and some deutered derivatives. J Mol Struct 321:187–195
58. Prates Ramalho JP, Costa Cabral BJ, Silva Fernandes FMS (1991) A Monte Carlo and transfer-matrix grid path-integral study of the vibrational structure of Br_2 in solid argon. Chem Phys Lett 184:53–60
59. Kirchoff WH, Johnson DR (1973) J Mol Spectrosc 45:159
60. Reed AE, Curtiss LA, Weinhold F (1988) Intermolecular interactions from a natural bond orbital, donor–acceptor viewpoint. Chem Rev 88:899–926
61. Bone RGA, Bader RFW (1996) Identifying and analyzing intermolecular bonding interactions in van der Waals molecules. J Phys Chem 100:10892–10911